






Experimental and numerical study of different mode-locking techniques in holmium fiber laser with a ring cavity

SERAFIMA FILATOVA,^{1,*}  VLADIMIR KAMYNNIN,¹  DMITRY KOROBKO,²  ANDREI FOTIADI,^{2,3} ARSENIY LOBANOV,¹ ANDREI ZVEREV,¹ PETR BALAKIN,¹ YURIY GLADUSH,⁴ DMITRY KRASNIKOV,⁴ ALBERT NASIBULIN,⁴ AND VLADIMIR TSVETKOV¹

¹Prokhorov General Physics Institute of the Russian Academy of Sciences, 38 Vavilov Str., Moscow, 119991, Russia

²Ulyanovsk State University, 42 Leo Tolstoy Str., Ulyanovsk, 432970, Russia

³Ioffe institute, 26 Politekhnicheskaya Str., St. Petersburg 194021, Russia

⁴Skolkovo Institute of Science and Technology, 3 Nobel Str., Moscow, 121205, Russia

*filatova@kapella.gpi.ru

Abstract: Experimental and numerical study has been performed for three techniques of mode-locking in all-fiber Holmium laser. We have compared the fundamental repetition rate pulsed generation for mode-locking based on: nonlinear polarization evolution, polymer-free single-walled carbon nanotubes, and hybrid mode-locking. Experimental and numerical simulation results demonstrated the shortest pulse duration and maximum spectrum width for mode-locking based on the nonlinear polarization evolution: 1.3 ps, 4.2 nm and 1.3 ps, 4.1 nm, respectively. The self-starting mode in this case can vary depending on external conditions in the experiment. In Ho-doped fiber laser with polymer-free single-walled carbon nanotubes mode-locking, the small modulation depth of saturable absorption leads to a long time period of stationary single-pulse lasing development (about 10^4 cavity roundtrips in simulation, and ≈ 5 s in the experiment). Both experimental and numerical studies have indicated that a Ho-doped fiber laser with hybrid mode-locking provides optimal generation, enabling self-starting and a relatively fast transition to stable single-pulse lasing (less than 1.5×10^3 cavity roundtrips in simulation, and ≈ 3 s in experiment). This study presents the first employment of polymer-free single-walled carbon nanotubes for hybrid mode-locking in a Ho-doped fiber laser.

© 2024 Optica Publishing Group under the terms of the [Optica Open Access Publishing Agreement](#)

1. Introduction

Ultrafast laser sources in 2- μm spectral range have been extensively researched throughout the years [1]. They are very promising for applications in material processing, laser surgery, biondiagnostics, molecular spectroscopy, mid-IR frequency combs, etc. [2–4]. They also can be used as the seed sources for nonlinear frequency conversion to produce a radiation above 2 μm and for mid-IR supercontinuum generation [5,6]. Furthermore, advances in material science have enabled remarkable progress in the generation of ultrashort pulses in the mid-IR range up to 3.5 μm [7,8].

Optical fiber is a promising active medium that allows designing compact and stable laser sources of ultrashort pulses with a good beam quality. The variety of commercially available fiber optic components makes it possible to build all-fiber systems that require minimal maintenance compared to solid-state lasers. One of the main methods of ultrashort pulse generation in fiber lasers is passive mode-locking, implemented while using artificial or material saturable absorbers (SA), which have been actively investigated over the years [9–11]. All these advantages in recent decades have contributed to significant progress in the development of the 2- μm ultrashort pulsed

fiber lasers based on thulium- (Tm^{3+}) and holmium-doped (Ho^{3+}) silica fibers [12]. To date, many publications have been devoted to the study of Tm-doped mode-locked fiber lasers. In these lasers pulse repetition rate ranging from tens of MHz to several GHz and pulse duration up to several fs have been achieved [13,14]. However, the longer wavelengths of Ho-doped fiber lasers (up to $2.2\ \mu\text{m}$ [15]) could be more optimal for some applications. For example, for sub-surface modification of silicon, effects on some biological tissues, for efficient operation in the atmospheric transmission window beyond $2.1\ \mu\text{m}$, and to achieve more efficient generation at longer wavelengths due to soliton self-shifting [5,16–19].

Various cavity schemes were considered for mode-locked Ho-doped fiber lasers to generate solitons, noise-like pulses, and dissipative solitons that turn into burst-like emission [20–23]. All these schemes were based on different saturable absorption mechanisms. These were carbon nanotubes [24], graphene [25], metallic carbon nanotubes [26], black phosphorus [27], semiconductor saturable absorption mirror (SESAM) [28], nonlinear polarization evolution (NPE) [29,30], nonlinear loop mirror [31], and hybrid mode-locking [32]. These studies on passively mode-locked Ho-doped fiber lasers were aimed on generation of ultrashort pulses with relatively low repetition-rate up to 100 MHz and energies in the range of 0.4–3 nJ. These output characteristics are not sufficient for such applications as material processing, material removal, and advanced communication systems. To improve efficiency in these applications, it is necessary to increase the pulse repetition rate or to generate pulse bursts [33–35].

A current focus of modern laser physics and technology is the GHz repetition rate of ultrashort pulses [36,37]. Passive harmonic mode-locking (HML) is the less technically challenging and more convenient method of achieving such repetition rate values [38,39]. It ensures uniform distribution of multiple ultrashort pulses in the ring fiber cavity under the pump power increasing. In addition to the study of harmonic mode-locking itself, methods for its control and stabilization are also actively investigated [40–42]. There are few works on HML for Ho-doped fiber lasers. In [28], HML with a pulse repetition rate of 290 MHz was demonstrated for a Ho-doped fiber laser mode-locked by a black phosphorus saturable absorber. Later, *Yang et al.* demonstrated 570 MHz HML in an all polarization-maintaining Ho-doped fiber laser based on the SESAM saturable absorber [43]. However, there has been no comprehensive analysis, including experimental, of how different mode-locking mechanisms affect high repetition rate pulsed generation. Before considering this issue, it is relevant to study the stability of lasers with different mode-locking types. Despite a significant influx of original research and reviews on the topic of ultrafast mid-infrared (MID-IR) laser systems [1,8,12,44], there has been no comprehensive experimental and numerical study of the self-start dynamics and estimation of the transition time to stable pulse generation in Ho-doped fiber lasers as a function of different mode-locking techniques. To date, only two types of mode-locking techniques have been experimentally compared under the same conditions in one cavity, based on single walled carbon nanotubes (SWCNT) in polymer matrix and hybrid mode-locking [45]. Recently, results of the numerical analysis of the hybrid mode-locking stability in a Ho-doped fiber laser with bulky elements [46] and the influence of SA parameters on the hybrid mode-locking performance of fiber lasers [47] have been published.

In this paper, we compared the fundamental repetition rate pulsed generation for three mode-locking techniques in the same cavity of a Ho-doped fiber laser. Experimental and numerical study of the generation optimum by mode-locking technique with a focus on the self-starting mode, including time estimation and probability of transition to pulse generation, has been performed. The obtained results are promising for further investigation of harmonic mode-locking in Ho-doped fiber lasers, as well as for the development of a stable self-starting and reproducible laser system to study the interaction of two-micron ultrashort pulsed radiation with biological tissues or other materials.

2. Materials and methods

2.1. Experimental setup

We have investigated three different techniques of passive mode-locking in the same ring cavity of a Ho-doped fiber laser. Figure 1(a) shows the experimental setup of this laser with mode-locking elements (MLE) corresponding to different mode-locking mechanisms, based on: nonlinear polarization evolution (NPE) (Fig. 1(b)) as artificial SA, polymer-free single walled carbon nanotubes (SWCNT) as material SA (Fig. 1(c)), and hybrid mode-locking, which combines the two previous mechanisms in a single cavity (Fig. 1(d)).

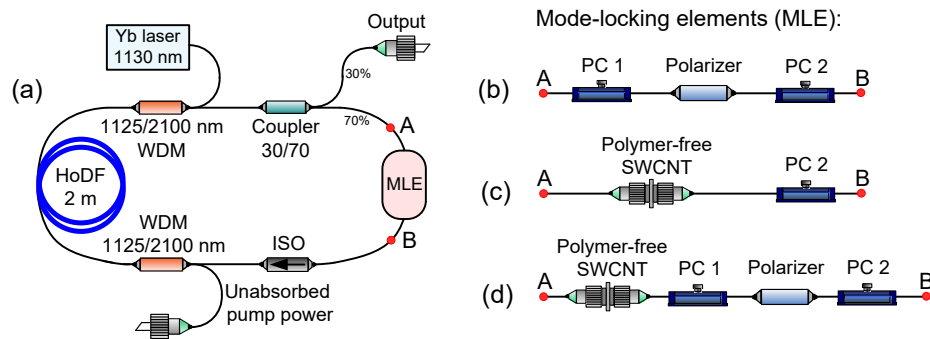


Fig. 1. (a) Experimental setup of the mode-locked Ho-doped fiber laser using different mode-locking elements (MLE) corresponding to different mode-locking mechanisms: (b) nonlinear polarization evolution (NPE), (c) polymer-free single walled carbon nanotubes (SWCNT), (d) hybrid mode-locking. HoDF – holmium-doped fiber, WDM – wavelength division multiplexer, ISO – isolator, PC 1, 2 – polarization controllers.

We have used silica-based optical fiber doped with Ho^{3+} ions to create the basic ring scheme of fiber laser. The concentration of active ions in the fiber core was $4 \times 10^{19} \text{ cm}^{-3}$, the core diameter was $11 \mu\text{m}$, and the numerical aperture was ~ 0.145 . The Ho-doped fiber was also doped with Al_2O_3 at a concentration of about 0.8 wt% and GeO_2 at a low concentration. The group velocity dispersion of a Ho-doped fiber around a wavelength of 2100 nm was estimated to be $\beta_2 \approx -0.112 \text{ ps}^2/\text{m}$. The ring laser cavity includes 2 m of Ho-doped fiber with counter-propagating pumping realized with continuous-wave (CW) Yb-doped fiber laser at a wavelength of 1130 nm through a 1125/2100 nm wavelength division multiplexer (WDM). The pump wavelength was determined by the holmium ions absorption spectrum at $^5\text{I}_8 \rightarrow ^5\text{I}_6$ transition, which have maximum at a wavelength of 1150 nm. However, there is a spectral dependence of the Yb-doped fiber laser efficiency, which decreases at wavelengths above 1130 nm [48]. We used a wavelength of Yb-doped fiber laser not exceeding 1130 nm for most experiments. It ensures sufficiently high generation efficiency and has a high absorption of holmium ions. The power of Yb-doped fiber laser was up to 6 W.

In addition to the active Ho-doped fiber, the laser cavity consisted of the fiber components based on a standard single mode (SM) silica fiber with a core diameter of $9 \mu\text{m}$. The group velocity dispersion of the SM fiber around a wavelength of 2100 nm was estimated to be $\beta_2 \approx -0.1 \text{ ps}^2/\text{m}$ [49]. The total cavity length varied from 9.5 to 11 m, depending on the used MLE. As noted above, the pump radiation was delivered to the cavity through a WDM 1125/2100 nm. An additional WDM 1125/2100 nm was used to output the unabsorbed pump power from the Ho-doped fiber laser cavity. Fiber isolator (ISO) operating at wavelengths above $2 \mu\text{m}$ ensured one direction of the laser radiation propagation. Insertion losses for ISO did not exceed 20%. Squeezer-based polarization controllers (PC) were used to adjust the intracavity polarization state. A fiber coupler with a coupling ratio of 30/70 was used as an output of the laser and

provided 30% output of laser power. The NPE mode-locking regime was implemented using a fiber polarizer placed in the laser cavity.

To achieve a mode-locking (ML) regime while using a material SA, we utilized polymer-free SWCNTs fixed between two angle-polished optical connectors (FC/APC) [50]. The SWCNTs were synthesized by the aerosol (floating catalyst) chemical vapor deposition technique [51] and were grown on the surface of iron-based catalyst particles via the Boudouard reaction. The catalyst was suspended (in the aerosol phase) in the CO atmosphere. The synthesis parameters were adjusted to achieve a mean diameter corresponding to the maximum of the optical transition around 1700–1900nm [52]. The thickness of SWCNT film was controlled by the collection time and was about 40 nm for this experiment corresponding to slightly more than 70% transmittance in the operating spectral range of 2050–2100 nm (Fig. 2(a)). The material was collected on a nitrocellulose filter from which SWCNT films can be transferred to the end of the FC/APC connector by a simple dry transfer technique [53]. The using this type of absorber is promising because it shows higher stability compared to composite SWCNT samples [54]. To realize hybrid mode-locking, we combined artificial (NPE) and material (SWCNT) saturable absorbers in a single laser cavity.

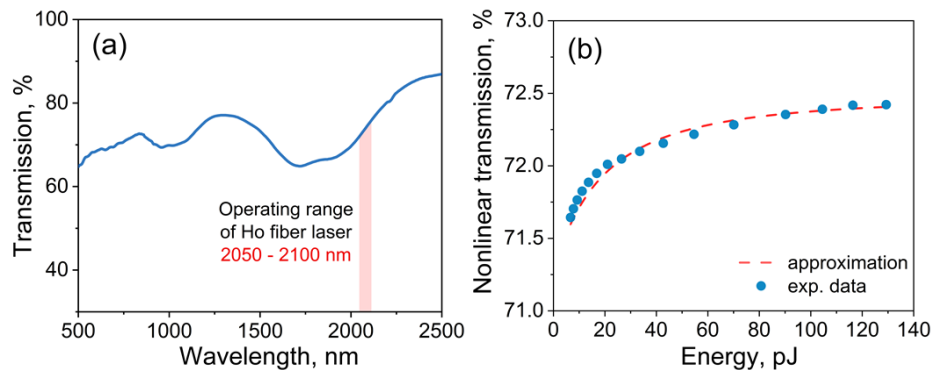


Fig. 2. (a) Transmission spectrum of the polymer-free SWCNT film; (b) Nonlinear transmission of the SWCNT thin film sample under the excitation of 1.6 ps pulses at 2080nm. Circles – experimental data, red dashed curve – approximation.

The nonlinear optical transmittance of SWCNT was measured using the conventional two-arm energy-dependent transmission technique [55]. A homemade Ho-doped fiber laser generating 1.6 ps pulsed radiation with a repetition rate of about 19 MHz at a center wavelength of 2080nm was used as the test laser source. The use of a variable optical attenuator allowed us to vary the laser radiation energy from 0 up to 130 pJ delivered to both arms (reference and test) formed by a 50/50 fiber coupler. The test arm contained SWCNT film sample fixed between two FC/APC connectors. We determined the nonlinear saturable absorption of the sample by comparing the pulse energy values at the outputs of the reference and test arms. Figure 2(b) shows the measured nonlinear transmission of SWCNT film sample. The experimental data were approximated using a simple formula as in [14,55]. The obtained values of modulation depths and non-saturable losses for SWCNT sample are $\approx 1\%$ and 27.5%, respectively.

An isolator was added at the laser output to prevent back reflection from entering the cavity. The laser radiation characteristics were measured after the isolator using the following equipment: an optical spectrum analyzer (Yokogawa AQ6375B, up to 2400 nm, resolution 0.1 nm), oscilloscope Tektronix MSO 64 (4 GHz) coupled with the photodetector EOT-5000 (12.5 GHz), radio frequency (RF) spectrum analyzer with 26.5 GHz bandwidth (Keysight 9020B), and scanning autocorrelator (Avesta AA-10DD-30ps).

2.2. Numerical model

To better interpret the experimental results, we have performed numerical simulations of the Ho-doped fiber laser with different types of mode-locking (ML) shown in Fig. 1 with some minor simplifications (for example, we simulated only one PC instead of the PC pair pointed in the Fig. 1(b,d)). The used numerical model is similar to the one described in [46,56,57]. The applied numerical model, uses some steady-state stationary values of the system parameters - gain coefficient and gain saturation energy of the active fiber, saturable losses and saturation power of the saturable absorber. This model is not applicable to describing the non-stationary laser turn-on (self-start) process accompanied by a gradual increase in pump power. Therefore, we do not directly link the experimental dynamics of the transient processes observed during laser self-start with the dynamics of the model describing the mode-locking process in a system with stationary parameters. The goal of the numerical simulation was to find a range of stationary parameters that would ensure successful mode locking with pulse characteristics close to the experimental ones. In the general case, light propagation in fiber elements has been described by a two-component nonlinear Schrödinger equation that takes into account the effects of birefringence, four-waves mixing, and spectrally limited amplification:

$$\frac{\partial A_x}{\partial z} - i\frac{\Delta\beta}{2}A_x + \delta\frac{\partial A_x}{\partial t} - i\frac{\beta_2}{2}\frac{\partial^2 A_x}{\partial t^2} - i\gamma\left(|A_x|^2 + \frac{2}{3}|A_y|^2\right)A_x - \frac{i}{3}\gamma A_x^* A_y^2 = \frac{gA_x}{2} + \frac{g}{2\Omega_g^2}\frac{\partial^2 A_x}{\partial t^2}, \quad (1a)$$

$$\frac{\partial A_y}{\partial z} + i\frac{\Delta\beta}{2}A_y - \delta\frac{\partial A_y}{\partial t} - i\frac{\beta_2}{2}\frac{\partial^2 A_y}{\partial t^2} - i\gamma\left(|A_y|^2 + \frac{2}{3}|A_x|^2\right)A_y - \frac{i}{3}\gamma A_y^* A_x^2 = \frac{gA_y}{2} + \frac{g}{2\Omega_g^2}\frac{\partial^2 A_y}{\partial t^2}, \quad (1b)$$

where A_i are the amplitudes of polarization components, $\Delta\beta=2\pi/L_B$ - difference of propagation constants due to birefringence in the fiber, L_B - birefringence length, $\delta=\Delta\beta/2\omega_0$ - difference of the group velocities of polarization components, β_2 - group velocity dispersion, γ - Kerr nonlinearity coefficient of the fiber. To simplify the numerical simulation, the values of the Kerr nonlinearity coefficient for HoDF and SMF were chosen to be the same. In the passive SMF the gain g is equal to zero but in the active fiber the saturated gain is averaged over the simulation window and is expressed as:

$$g(z) = g_0 \left(1 + \frac{1}{E_g} \int_0^{\tau_{win}} (|A_x(z,t)|^2 + |A_y(z,t)|^2) dt \right)^{-1}, \quad (2)$$

where g_0 is a small signal gain factor and E_g is the gain saturation energy determined by the pump power, τ_{win} is the width of the simulation window. The gain spectral filtering is centered at $\lambda_0=2070\text{nm}$ and employed in parabolic approximation with the full width at half maximum (FWHM) gain line bandwidth Ω_g .

The PC is placed so that it divides the length of passive SM fiber in a ratio of 1:3. PC transforms the light to an elliptical polarization state. The transformation is described by the transfer matrix:

$$\begin{pmatrix} \cos \theta & -\sin \theta \exp(-i\Delta\phi) \\ \sin \theta \exp i\Delta\phi & \cos \theta \end{pmatrix}, \quad (3)$$

where θ - the PC rotation angle, $\Delta\phi$ - the phase difference between the components contributed by the PC. A polarizer returns the light to a linear polarization state $A_x = A_x \cos \varphi + A_y \sin \varphi$, where φ - orientation angle of the polarizer. Thus, in configurations that include a polarizer, light propagation in the section between polarizer and PC is described by a standard one-component nonlinear Schrödinger equation.

This work focuses on the three mode-locking types based on the NPE, SWCNT, and hybrid, which combines the previous two. In the case of material SA mode-locking based on SWCNT its action is described by a transfer function:

$$A'_i = A_i \sqrt{1 - \alpha_{ns} - \alpha_s}, \quad (4)$$

where $\alpha_s = \alpha_{s0} \exp(-(|A_x|^2 + |A_y|^2)/P_s)$ is the SWCNT saturated losses, α_{s0} is the modulation depth, P_s is the saturation peak power, and α_{ns} is the non-saturable losses. The same sample of polymer-free SWCNTs was used in the schemes with hybrid mode-locking and material SA. The effect of modulation is important in mode-locked fiber lasers, as well as recovery time of SA [58,59]. Typically, NPE based on the Kerr effect has a response time of a few femtoseconds and SWCNT has a response time of several hundred femtoseconds and more.

Table 1 presents parameter values used in the numerical simulation. Since the length of SM fiber varied (7.5-9 m) depending on the used MLEs, an approximate average SM fiber length of 8 m was considered in the numerical simulation. All the linear losses experienced by the signal inside the cavity are taken into account as the local losses in the output coupler with power transmission coefficient equal to 1/2.

Table 1. Values of parameters used in the numerical simulation.

Ho-doped fiber					
β_2 (ps ² m ⁻¹)	γ (W ⁻¹ m ⁻¹)	g_0 (m ⁻¹)	$\frac{\Omega_g}{2\pi}$ (THz)	E_g (pJ)	l_a (m)
-0.11	0.0011	2	2.66	180	2
SMF			SWCNT		
β_2 (ps ² m ⁻¹)	γ (W ⁻¹ m ⁻¹)	l_{SMF} (m)	α_{ns}	α_{s0}	P_s (W)
-0.1	0.0011	8	0.28	0.01	70
General parameters					
L_B (m)	θ (rad)	$\Delta\phi$ (rad)	φ (rad)	τ_{win} (ps)	
0.5	0.3	$(\frac{\pi}{2}..\pi)$	2.45	404.8	

3. Experimental results

3.1. NPE mode-locking

Figure 1(a) shows the scheme of Ho-doped fiber laser, which employs the MLE such as nonlinear polarization evolution (Fig. 1(b)) based on the nonlinear optical Kerr effect in fibers. To achieve nonlinear polarization evolution, we added an optical polarizer to the cavity of Ho-doped fiber laser. Polarizer with polarization controllers allow tuning the transmission state to minimize losses of the higher intensity components and maximize absorption of the lowest ones. This approach refers to an artificial saturable absorber that possesses a fast relaxation time of approximately 5 fs. Although this effect is considered spectrally independent, the lower effective nonlinearity of silica fibers in the 2 μ m spectral range affects the nonlinear response and contributes to a higher mode-locking threshold, in contrast to material SAs [12].

The total laser cavity length was ≈ 10.2 m and consisted of a 2 m long active Ho-doped fiber and ≈ 8.2 m long of standard single-mode fiber. The net cavity dispersion of laser cavity was estimated to be about -1.08 ps². The radiation output from the cavity was carried out through the 30% output of the fiber coupler. The laser generation threshold was at a pump power of 0.73 W, and the mode-locking threshold was at a pump power of 0.82 W.

Figure 3 shows the pulsed radiation characteristics measured at a pump power of 0.85 W. The average output power was 6 mW, and the unabsorbed pump power was 7.2 mW. As can be seen in Fig. 3(a), the central emission wavelength is 2069 nm, and the spectrum width at half-maximum

is 4.2 nm. Figure 3(b) displays the map of time-dependent spectral stability measurements for 1 hour. Based on these data, Fig. 3(a) contains two spectra at the start (1 min) and the end (62 min) of the measurements to demonstrate spectral detuning. The optical spectrum has a typical shape with sidebands determined by periodic spectral interference between the soliton wave and a co-propagating dispersive wave. Figure 3(c) shows the radio frequency (RF) spectrum at the fundamental repetition rate of 20.4 MHz with a signal-to-noise ratio of about 65 dB. The repetition rate corresponds to the laser cavity length. The autocorrelation trace of the laser pulse with a theoretical sech^2 fitting is shown in Fig. 3(d). The measured pulse duration of 1.3 ps corresponds to a time-bandwidth product of 0.382, indicating a slight chirping of the pulse. The laser pulse energy was estimated to be 0.3 nJ, and the peak power ≈ 231 W.

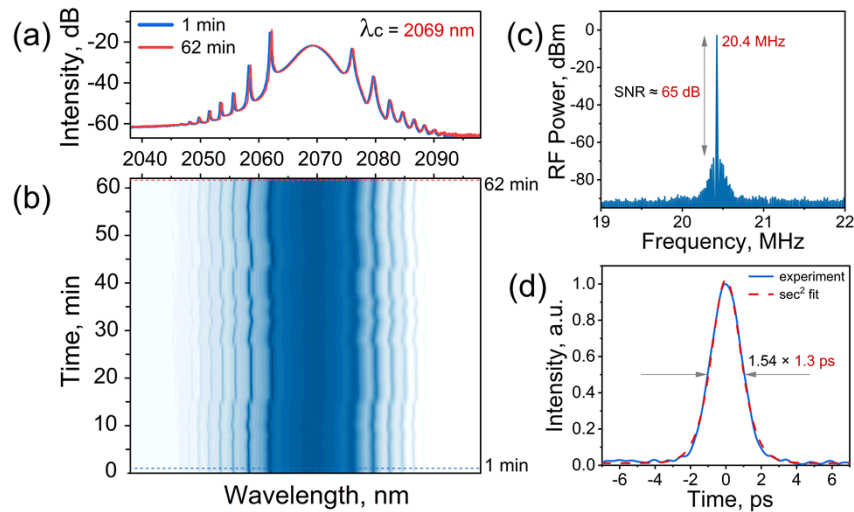


Fig. 3. Radiation characteristics of the mode-locked Ho-doped fiber laser utilized NPE effect: (a) optical spectra, (b) map of time-dependent spectral stability for 62 minutes, (c) RF spectrum (3 MHz span, 50 Hz resolution bandwidth), (d) pulse autocorrelation function.

3.2. Polymer-free SWCNT mode-locking

Figure 1(a) shows the scheme of the Ho-doped fiber laser, which employs the MLE shown in Fig. 1(c). The polymer-free single-walled carbon nanotubes described above were used as material SA to achieve the mode-locking regime. In contrast to the NPE effect, the SWCNT saturable absorber has a longer relaxation time of about 1 ps [11]. The properties of SWCNT as SA are affected by several parameters, including diameter, chirality, length, and orientation. These parameters are predetermined by the synthesis method and post-processing stage [60]. The degree of SWCNT orientation determines their polarization sensitivity. For operations at wavelengths above 1.9 μm , the diameter of SWCNT must be increased to match the bandgap. An increase in diameter leads to more defects and higher losses, which limits the maximum operating wavelength. Alternative fabrication methods of SWCNT, such as the aerosol (floating catalyst) chemical vapor deposition method, allow extending the operating spectral range of SWCNTs while maintaining their defect-free quality [51].

The investigated Ho-doped fiber laser cavities utilized the same sample of polymer-free SWCNT fixed between FC/APC optical connectors. Optical connectors with SWCNT were placed in the laser cavity between the coupler, which outputs a part of radiation, and the isolator to reduce the power density passing through SWCNT. In this laser scheme, we have used only one polarization controller to adjust the polarization state. It was placed after optical connectors

with the SWCNT along the radiation propagation path. The total laser cavity length was ≈ 9.5 m and consisted of a 2 m long active Ho-doped fiber and ≈ 7.5 m long of standard single-mode fiber. The net cavity dispersion of the laser cavity was estimated to be about -1 ps². The radiation output from the cavity was carried out through the 30% output of the fiber coupler. The laser generation threshold was at a pump power of 0.7 W, and the mode-locking threshold was at a pump power of 0.8 W.

Figure 4 shows the pulsed radiation characteristics measured at a pump power of 0.85 W. The average output power was 6.5 mW, and the unabsorbed pump power was 7 mW. As can be seen in Fig. 4(a), the central emission wavelength is 2076 nm, and the spectrum width at half-maximum is 3.5 nm. Figure 4(b) displays the map of time-dependent spectral stability measurements for 1 hour. Based on these data, Fig. 4(a) contains two spectra at the start (1 min) and the end (62 min) of the measurements to demonstrate spectral detuning. The optical spectrum has a typical shape with Kelly sidebands. As can be seen, there are additional Kelly sidebands, detuned from the main ones. It can be assumed that the absence of a polarization state selector results in the presence of two solitons with orthogonal polarization state that are superimposed on each other. Figure 4(c) shows the RF-spectrum at the fundamental repetition rate of 21.8 MHz with a signal-to-noise ratio of about 67 dB. The repetition rate corresponds to the laser cavity length. The autocorrelation trace of the laser pulse with a theoretical sech² fitting is shown in Fig. 4(d). The measured pulse duration of 1.4 ps corresponds to a time-bandwidth product of 0.341, indicating a slight chirping of the pulse. The laser pulse energy was estimated to be 0.3 nJ, and the peak power ≈ 214 W.

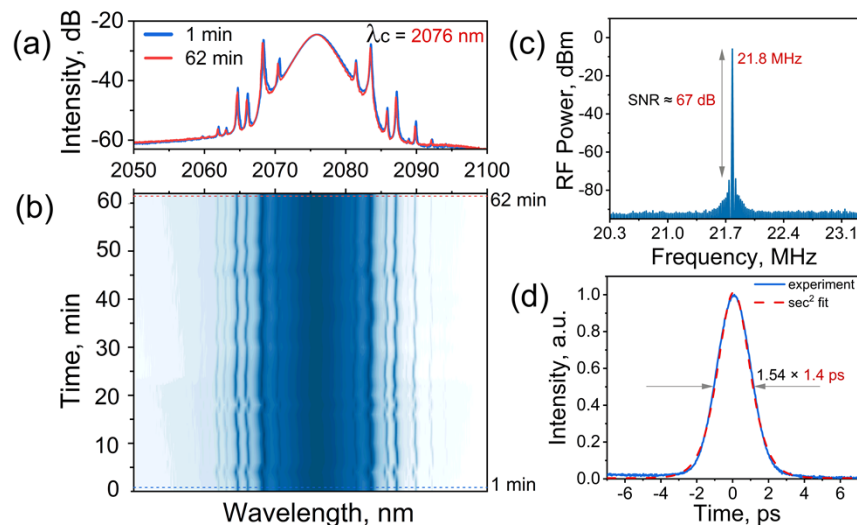


Fig. 4. Radiation characteristics of the mode-locked Ho-doped fiber laser utilized polymer-free SWCNT: (a) optical spectra, (b) map of time-dependent spectral stability for 62 minutes, (c) RF spectrum (3 MHz span, 50 Hz resolution bandwidth), (d) pulse autocorrelation function.

3.3. Hybrid mode-locking

Figure 1(a) shows the scheme of Ho-doped fiber laser, which employs hybrid mode-locking (Fig. 1(d)). This approach consists of combining fast and slow saturable absorbers in the laser cavity. SWCNT, as material SAs, contribute to longer pulse durations, have a lower damage threshold, and can degrade over time (depending on the SWCNT type). At the same time, they have a low self-start threshold for generating ultrashort pulses. Artificial SAs such as NPE based

on the nonlinear optical Kerr effect allow the generation of high-quality ultrashort pulses without a pedestal. However, they often lack self-starting capabilities and have lower nonlinearity in the 2 μm spectral range. Therefore, when both types of SAs are combined in the same laser cavity, the material SA initiates and stabilizes the pulse formation, while the artificial SA shapes and cleans the pulse width to shorter durations.

To achieve hybrid mode-locking, SWCNT and a polarizer with a pair of PCs were utilized in the cavity of a Ho-doped fiber laser. We used the same sample of polymer-free SWCNT fixed between two FC/APC connectors in all experiments. The total laser cavity length was ≈ 11 m and consisted of a 2 m long active Ho-doped fiber and ≈ 9 m long of standard single-mode fiber. The net cavity dispersion of the laser cavity was estimated to be about -1.17 ps². The radiation output from the cavity was carried out through the 30% output of the fiber coupler. The laser generation threshold was at a pump power of 0.8 W, and the mode-locking threshold was at a pump power of 0.84 W.

Figure 5 shows the pulsed radiation characteristics measured at a pump power of 0.85 W. The average output power was 4 mW, and the unabsorbed pump power was 8.3 mW. As can be seen in Fig. 5(a), the central emission wavelength is 2077 nm, and the spectrum width at half-maximum is 3.6 nm. Figure 5(b) displays the map of time-dependent spectral stability measurements for 1 hour. Based on these data, Fig. 5(a) contains two spectra at the start (1 min) and the end (62 min) of the measurements to demonstrate spectral detuning. The optical spectrum has a typical shape with Kelly sidebands. Figure 5(c) shows the RF-spectrum at the fundamental repetition rate of 19 MHz with a signal-to-noise ratio of about 64 dB. The repetition rate corresponds to the laser cavity length. The autocorrelation trace of the laser pulse with a theoretical sech² fitting is shown in Fig. 5(d). The measured pulse duration of 1.5 ps corresponds to a time-bandwidth product of 0.375. The laser pulse energy was estimated to be 0.21 nJ, and the peak power ≈ 140 W.

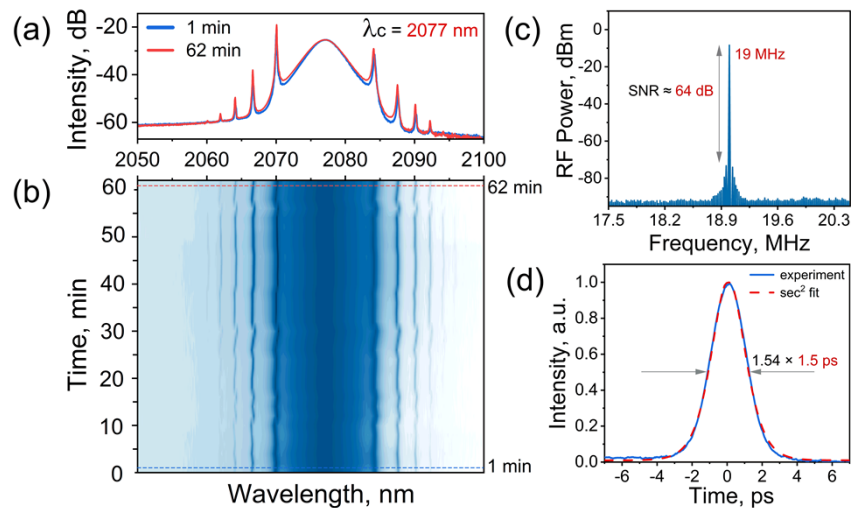


Fig. 5. Radiation characteristics of the mode-locked Ho-doped fiber laser utilized both NPE effect and polymer-free SWCNT: (a) optical spectra, (b) map of time-dependent spectral stability for 62 minutes, (c) RF spectrum (3 MHz span, 50 Hz resolution bandwidth), (d) pulse autocorrelation function.

We experimentally investigated three different mode-locking techniques in a Ho-doped fiber laser, based on: nonlinear polarization evolution (NPE) as artificial SA, polymer-free single walled carbon nanotubes (SWCNT) as material SA, and hybrid mode-locking, which combines the two previous SAs in one cavity. Table 2 summarizes the experimentally obtained laser generation

characteristics depending on the different ML types at the same pump power of 0.85 W. The pulse repetition rate differs slightly depending on the used MLE. As can be seen, the shortest pulse duration and the highest pulse energy were achieved for NPE- and SWCNT-based mode-locking. Stable self-start of ML regime was observed only for SWCNT and hybrid mode-locking. The results of time-dependent spectral stability study showed that NPE- or SWCNT- based ML had more wavelength variations during operation compared with hybrid mode-locking. That is, combining two types of absorbers, artificial and material, in a cavity allows one to overcome their shortcomings and improve the generation mode.

Table 2. The experimentally obtained characteristics of laser radiation as a function of different mode-locking (ML) types used in the Ho-doped fiber laser: nGVD – net group velocity dispersion of the cavity, λ_c – central wavelength, FWHM – optical spectrum bandwidth at half maximum, Frep – pulse repetition rate, Pp – pump power, Pavg – average output power, τ – pulse duration, E – pulse energy, TBP – time-bandwidth product.

ML type	Cavity length [m]	nGVD [ps ²]	λ_c [nm]	FWHM [nm]	Frep [MHz]	Pp [W]	Pavg [mW]	τ [ps]	E [nJ]	TBP	Self-start
NPE	≈ 10.2	−1.08	2069	4.2	20.4	0.85	6	1.3	0.3	0.382	variably
SWCNT	≈ 9.5	−1	2076	3.5	21.8	0.85	6.5	1.4	0.3	0.341	Yes
Hybrid	≈ 11	−1.17	2077	3.6	19	0.85	4	1.5	0.21	0.375	Yes

4. Numerical simulation results and discussion

We investigated the transition of laser system into the stationary single pulse generation mode using low-amplitude Gaussian noise as initial conditions. In all considered cases with three different ML types, the laser system successfully switched to this mode in approximately 500–10⁴ cavity roundtrips.

When describing the simulation results of a mode-locked laser that utilizes the NPE effect, it is important to consider the formation of a birefringent Lyot filter in the ring fiber cavity. In this model, it is formed within a $3/4l_{SMF}$ long segment of fiber located between the polarization controller and the polarizer. And its transmittance is equal [61]:

$$T(\lambda) = (\cos \theta \cos \varphi)^2 + (\sin \theta \sin \varphi)^2 + 1/2 \sin 2\theta \sin 2\varphi \cos \left(\Delta\varphi - \frac{3}{4} \frac{l_{SMF}}{L_B} \frac{\lambda_0}{\lambda} \right), \quad (5)$$

where the parameter $\Delta\varphi$ is the birefringence introduced by the polarization controller (possibly together with other cavity components in this segment), which can be varied by adjustment. A key feature of the NPE mode-locking is the increasing of pulse transmittance compared to the linear background. This occurs due to the nonlinear addition to the phase $\Delta\varphi \rightarrow \Delta\varphi + \Delta\varphi_{NL}$. Figure 6 shows the numerical simulation results of the mode-locked Ho-doped fiber laser utilized the NPE effect. This figure displays the pulse envelope and spectrum of the stationary single-pulse generation. The spectral dependences in Fig. 6(b,c) show 2 options of the joint position of the pulse spectrum and the linear transmission of the Lyot filter (5) in the fiber cavity. These options correspond to different settings of the parameter $\Delta\varphi$. As can be seen, the simulation results for the $\Delta\varphi = \pi$ settings closely match the experimental results.

Figure 7 shows the pulse envelope and spectrum of the stationary single-pulse generation of Ho-doped fiber laser utilized SWCNT saturable absorber. In this case, the central generation wavelength is close to the position of maximum gain in the Ho-doped fiber, which is fixed in the model at a wavelength of $\lambda_c = 2075\text{nm}$ (Fig. 7(b)). The simulation confirms the assumption that the pulse of a Ho-doped fiber laser with SWCNT saturable absorber is the sum of two orthogonally polarized solitons that trap each other and propagate as a single vector soliton unit [62,63]. Figure 7(c) shows the separate spectra of pulsed radiation with two polarization components.

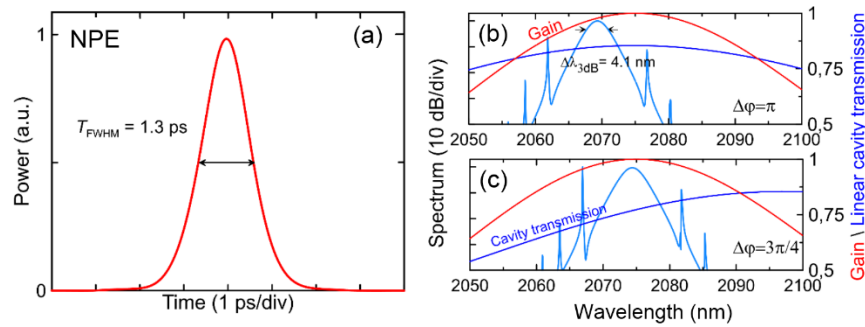


Fig. 6. Numerical simulation results of the mode-locked Ho-doped fiber laser utilized the NPE effect: (a) pulse envelope, (b) and (c) show the possible shift of the spectrum that occurs when the phase difference between two polarization components is varied, e.g. by the PC adjusting.

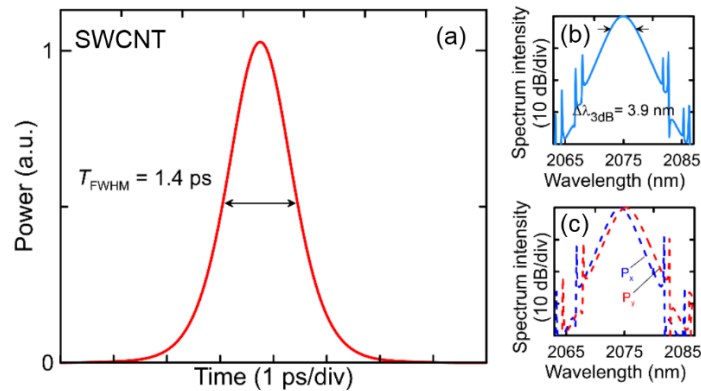


Fig. 7. Numerical simulation results of the mode-locked Ho-doped fiber laser utilizing the polymer-free SWCNT saturable absorber: (a) pulse envelope, (b) pulsed radiation spectrum representing the sum of two polarization components, (c) separate spectra of pulsed radiation with two polarization components.

Finally, the numerical simulation results for Ho-doped fiber laser with hybrid mode-locking (NPE + SWCNT) are presented (Fig. 8). It is worth noting that there is no fundamental difference between the results obtained for this case and for Ho-doped fiber laser with NPE mode-locking only. The central wavelength of the pulsed radiation in the stationary single-pulse generation mode can also be adjusted by changing the parameter $\Delta\varphi$. The simulation results obtained with $\Delta\varphi=2.1$ are close to the experimental data (Fig. 8(b)). An important difference, however, is that the introduction of SWCNT causes increased losses in the cavity, resulting in a slight pulse duration increasing and decrease in a spectral width.

As can be seen, the numerical simulation and experimental results are very close. Numerical simulation showed the longest pulse duration (1.6 ps) and the minimum spectrum width at half maximum (3.7 nm) for hybrid mode-locking due to the increased loss level in this cavity. However, the experimental results showed the minimum spectrum width (3.5 nm) for SWCNT mode-locking. Which was insignificantly different from the spectrum width in the case of hybrid ML (3.6 nm). Experimental and numerical simulation results demonstrated the shortest pulse duration and maximum spectrum width at half-maximum for NPE mode-locking: 1.3 ps, 4.2 nm and 1.3 ps, 4.1 nm, respectively.

The self-starting features of Ho-doped fiber laser with different ML techniques were analyzed. The numerical simulation considered this issue by using a variable birefringence length parameter L_B . The results showed that mode-locking self-start is independent of the L_B parameter when material SA based on the polymer-free SWCNT is used. This is due to the absence of polarization state selector in this cavity configuration. This indicates that the laser is capable of self-starting despite significant variations in external conditions. However, as previously mentioned, the small modulation depth of saturable absorption leads to a long period of stationary mode-locking formation – about 10^4 cavity roundtrips and more. The experiments also detected this feature. Figure 9(a) displays one of the best experimental oscilloscope trace of the laser self-start process. In this case a Ho-doped fiber laser was able to self-start, but with a longer time (about 5 s) of single-pulse mode formation compared with other ML techniques. During this time transient processes occur, which may be accompanied by the generation of giant pulses. This can lead to undesirable damage of the SWCNTs. Therefore, it is important to optimize and appropriately select the parameters of saturable absorber. Numerical simulations have shown that for NPE mode-locking the most successful transition to the pulse mode occurs when the L_B parameter value is within the range of ≈ 0.5 – 4.5 m. The addition of SWCNT to the cavity with NPE extends this range to ≈ 0.1 – 5 m (this study considers achieving stationary pulse generation in less than 1.5×10^3 cavity roundtrips a successful realization.). The wide range of possible L_B values confirm the high probability of mode-locking self-start in Ho-doped fiber laser. Experimental analysis showed that the self-starting probability of NPE mode-locking can vary depending on external conditions. Thus, we did not observe self-start at every laser launch. Another disadvantage of this ML technique is the need to adjust the polarization controllers to correct the polarization state, which sometimes takes a long time. Combining two saturable absorbers NPE and SWCNT in the cavity, indeed promoted the repetitive self-start of the Ho-doped fiber laser. Figure 9(b) displays the experimental oscilloscope trace of the laser self-starting process. As can be seen, the transition time to stationary single-pulse generation takes slightly more than 3 s, which is 1.5 times faster than for SWCNT ML. Thus, experiment and simulation showed that this approach provides the fastest transition to the stationary single-pulse generation mode. This means that the hybrid mode-locking regime is robust to changes in external conditions and reduces the probability of SWCNT damage during transient processes. The transition time to stationary single-pulse generation differs between the experiment and simulation. The long transition time of Ho-doped fiber laser to the stationary single-pulse lasing in the experiment is related to the warm-up time of the Yb pump laser. The reason for this is that the Yb-doped fiber laser is pumped by a multimode, unstabilized laser diode.

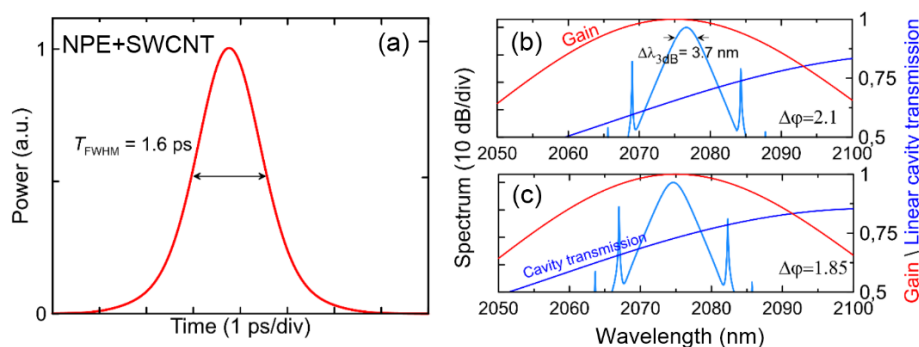


Fig. 8. Numerical simulation results of the mode-locked Ho-doped fiber laser utilized both NPE effect and polymer-free SWCNT saturable absorber: (a) pulse envelope, (b) and (c) show the possible shift of the spectrum that occurs when the phase difference between two polarization components is varied, e.g. by the PC adjusting.

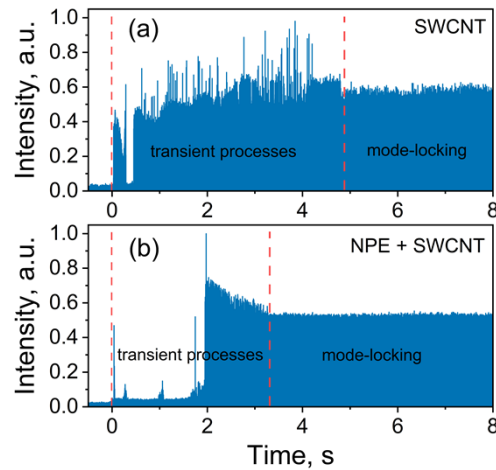


Fig. 9. The experimental oscilloscope traces of the self-start process for Ho-doped fiber laser with different ML types: (a) based on the polymer-free SWCNT; (b) hybrid ML (NPE + SWCNT).

Both experimental and numerical studies have indicated that the optimal generation in a Ho-doped fiber laser, which enables self-starting and fast transition to stable single-pulse generation, is achieved using hybrid ML.

5. Conclusion

In this work, we have compared the fundamental repetition rate pulsed generation for three mode-locking techniques in the same cavity of Ho-doped fiber laser based on: nonlinear polarization evolution as artificial SA, polymer-free SWCNT thin film as a material SA, and hybrid mode-locking, which combines the two previous mechanisms in the cavity. Experimental and numerical study of the generation optimum by mode-locking technique within the same cavity with a focus on the self-starting mode, including time estimation and probability of transition to pulse generation, has been performed.

In the experiment, the shortest pulse duration and the highest pulse energy were achieved for NPE- (1.3 ps, 0.3 nJ) and polymer-free SWCNT-based (1.4 ps, 0.3 nJ) mode-locking. Results of the time-dependent spectral stability study showed that NPE- or SWCNT-based ML had more wavelength variations during operation compared with hybrid ML. Numerical simulation results demonstrated the shortest pulse duration and maximum spectrum width for NPE mode-locking: 1.3 ps, 4.1 nm. Experimental analysis showed that the self-starting of NPE mode-locking can vary depending on external conditions. The lack of a polarization state selector in the Ho-doped fiber laser with SWCNT-based ML results in the formation of two orthogonally polarized solitons that mutually trap each other, propagating as a single vector soliton unit. This contributes to the laser's ability to self-starting despite the significant changes in external conditions. However, the small modulation depth of saturable absorption leads to a long time period of stationary single-pulse lasing development, about 10^4 cavity roundtrips and more in simulation, and about 5 s in experiment.

Both experimental and numerical studies have indicated that Ho-doped fiber laser with hybrid mode-locking provides optimal lasing, enabling self-starting and a faster transition to stable single-pulse generation (less than 1.5×10^3 cavity roundtrips in simulation, and about 3 s in experiment). This study presents the first using of polymer-free SWCNT for hybrid mode-locking in a Ho-doped fiber laser.

Funding. Russian Science Foundation (22-72-00126, 23-79-30017).

Disclosures. The authors declare no conflicts of interest.

Data availability. Data underlying the results presented in this paper are not publicly available at this time but may be obtained from the authors upon reasonable request.

References

1. J. Ma, Z. Qin, G. Xie, *et al.*, “Review of mid-infrared mode-locked laser sources in the 2.0 μm –3.5 μm spectral region,” *Appl. Phys. Rev.* **6**(2), 021317 (2019).
2. R. R. Gattass and E. Mazur, “Femtosecond laser micromachining in transparent materials,” *Nat. Photonics* **2**(4), 219–225 (2008).
3. M. S. Kopyeva, S. A. Filatova, V. A. Kamynin, *et al.*, “Ex Vivo Exposure to Soft Biological Tissues by the 2- μm All-Fiber Ultrafast Holmium Laser System,” *Appl. Sci.* **12**(8), 3825 (2022).
4. S. Xing, A. S. Kowligy, D. M. B. Lesko, *et al.*, “All-fiber frequency comb at 2 μm providing 1.4-cycle pulses,” *Opt. Lett.* **45**(9), 2660 (2020).
5. V. A. Kamynin, S. A. Filatova, B. I. Denker, *et al.*, “Tm³⁺-doped tellurite fiber weak signal amplifier at a wavelength of 2.27 μm ,” *Results Phys.* **27**, 104512 (2021).
6. V. Voropaev, S. Xie, A. Donodin, *et al.*, “Octave-Spanning Supercontinuum Generation in As₂S₃-Silica Hybrid Waveguides Pumped by Thulium-Doped Fiber Laser,” *J. Lightwave Technol.* **41**(15), 5116–5122 (2023).
7. E. A. Anashkina, “Laser Sources Based on Rare-Earth Ion Doped Tellurite Glass Fibers and Microspheres,” *Fibers* **8**(5), 30 (2020).
8. X. Li, X. Huang, X. Hu, *et al.*, “Recent progress on mid-infrared pulsed fiber lasers and the applications,” *Opt. Laser Technol.* **158**, 108898 (2023).
9. S. M. Kobtsev, “Artificial saturable absorbers for ultrafast fibre lasers,” *Opt. Fiber Technol.* **68**, 102764 (2022).
10. T. Jiang, K. Yin, C. Wang, *et al.*, “Ultrafast fiber lasers mode-locked by two-dimensional materials: review and prospect,” *Photonics Res.* **8**(1), 78–90 (2020).
11. S. Yamashita, “Nonlinear optics in carbon nanotube, graphene, and related 2D materials,” *APL Photonics* **4**(3), 034301 (2019).
12. D. C. Kirsch, S. Chen, R. Sidharthan, *et al.*, “Short-wave IR ultrafast fiber laser systems: Current challenges and prospective applications,” *J. Appl. Phys.* **128**(18), 180906 (2020).
13. J. Shang, S. Zhao, Y. Liu, *et al.*, “Gigahertz-repetition rate, high power, ultrafast Tm-doped fiber laser source,” *Opt. Laser Technol.* **153**, 108206 (2022).
14. D. C. Kirsch, A. Bednyakova, P. Varak, *et al.*, “Gain-controlled broadband tuneability in self-mode-locked Thulium-doped fibre laser,” *Commun. Phys* **5**(1), 219 (2022).
15. L. G. Holmen, P. C. Shardlow, P. Barua, *et al.*, “Tunable holmium-doped fiber laser with multiwatt operation from 2025 nm to 2200 nm,” *Opt. Lett.* **44**(17), 4131 (2019).
16. R. A. Richter, N. Tolstik, S. Rigaud, *et al.*, “Sub-surface modifications in silicon with ultra-short pulsed lasers above 2 μm ,” *J. Opt. Soc. Am. B* **37**(9), 2543–2556 (2020).
17. S. A. Filatova, I. A. Shcherbakov, and V. B. Tsvetkov, “Optical properties of animal tissues in the wavelength range from 350 to 2600 nm,” *J. Biomed. Opt.* **22**(3), 035009 (2017).
18. S. Tomilov, M. Tarabrin, V. Lazarev, *et al.*, “Broadband tunable mid-IR Cr²⁺:CdSe lasers for medical applications,” *Proc. SPIE* **10717**, 32–36 (2018).
19. A. Hemming, N. Simakov, J. Haub, *et al.*, “A review of recent progress in holmium-doped silica fibre sources,” *Opt. Fiber Technol.* **20**(6), 621–630 (2014).
20. M. Pawliszewska, A. Dużyńska, M. Zdrojek, *et al.*, “Wavelength- and dispersion-tunable ultrafast holmium-doped fiber laser with dual-color operation,” *Opt. Lett.* **45**(4), 956–959 (2020).
21. S. A. Filatova, V. A. Kamynin, Y. G. Gladush, *et al.*, “Dumbbell-Shaped Ho-Doped Fiber Laser Mode-Locked by Polymer-Free Single-Walled Carbon Nanotubes Saturable Absorber,” *Nanomaterials* **13**(10), 1581 (2023).
22. J. Wang, J. Han, J. He, *et al.*, “High-energy mode-locked holmium-doped fiber laser operating in noise-like pulse regime,” *Opt. Lett.* **44**(18), 4491–4494 (2019).
23. J. Zhao, J. Zhou, L. Li, *et al.*, “Dissipative soliton resonance and its depression into burst-like emission in a holmium-doped fiber laser with large normal dispersion,” *Opt. Lett.* **44**(10), 2414–2417 (2019).
24. A. Y. Chamorovskiy, A. V. Marakulin, A. S. Kurkov, *et al.*, “Tunable Ho-doped soliton fiber laser mode-locked by carbon nanotube saturable absorber,” *Laser Phys. Lett.* **9**(8), 602–606 (2012).
25. J. Sotor, M. Pawliszewska, G. Sobon, *et al.*, “All-fiber Ho-doped mode-locked oscillator based on a graphene saturable absorber,” *Opt. Lett.* **41**(11), 2592–2595 (2016).
26. M. Pawliszewska, A. Dużyńska, M. Zdrojek, *et al.*, “Metallic carbon nanotube-based saturable absorbers for holmium-doped fiber lasers,” *Opt. Express* **27**(8), 11361–11369 (2019).
27. M. Pawliszewska, Y. Ge, Z. Li, *et al.*, “Fundamental and harmonic mode-locking at 2.1 μm with black phosphorus saturable absorber,” *Opt. Express* **25**(15), 16916–16921 (2017).
28. M. Hinkelmann, D. Wandt, U. Morgner, *et al.*, “Mode-locked Ho-doped laser with subsequent diode-pumped amplifier in an all-fiber design operating at 2052nm,” *Opt. Express* **25**(17), 20522–20529 (2017).
29. P. Li, A. Ruehl, C. Bransley, *et al.*, “Low noise, tunable Ho: fiber soliton oscillator for Ho:YLF amplifier seeding,” *Laser Phys. Lett.* **13**(6), 065104 (2016).

30. S. A. Filatova, V. A. Kamynin, I. V. Zhlyukova, *et al.*, “All-fiber passively mode-locked Ho-laser pumped by ytterbium fiber laser,” *Laser Phys. Lett.* **13**(11), 115103 (2016).
31. J. Zhao, J. Zhou, Y. Jiang, *et al.*, “Nonlinear Absorbing-Loop Mirror in a Holmium-Doped Fiber Laser,” *J. Lightwave Technol.* **38**(21), 6069–6075 (2020).
32. S. A. Filatova, V. A. Kamynin, N. R. Arutyunyan, *et al.*, “Hybrid mode locking of an all-fiber holmium laser,” *J. Opt. Soc. Am. B* **35**(12), 3122–3125 (2018).
33. C. Kerse, H. Kalaycıoğlu, P. Elahi, *et al.*, “Ablation-cooled material removal with ultrafast bursts of pulses,” *Nature* **537**(7618), 84–88 (2016).
34. D. J. Förster, B. Jäggi, A. Michalowski, *et al.*, “Review on Experimental and Theoretical Investigations of Ultra-Short Pulsed Laser Ablation of Metals with Burst Pulses,” *Materials* **14**(12), 3331 (2021).
35. P. Lin, T. Wang, W. Ma, *et al.*, “2- μm Free-Space Data Transmission Based on an Actively Mode-Locked Holmium-Doped Fiber Laser,” *IEEE Photonics Technol. Lett.* **32**(5), 223–226 (2020).
36. J. Bogusławski, G. Soboń, R. Zybala, *et al.*, “Towards an optimum saturable absorber for the multi-gigahertz harmonic mode locking of fiber lasers,” *Photonics Res.* **7**(9), 1094–1100 (2019).
37. W. Ma, T. Wang, F. Wang, *et al.*, “2.07- μm , 10-GHz Repetition Rate, Multi-Wavelength Actively Mode-Locked Fiber Laser,” *IEEE Photonics Technol. Lett.* **31**(3), 242–245 (2019).
38. A. B. Grudinin and S. Gray, “Passive harmonic mode locking in soliton fiber lasers,” *J. Opt. Soc. Am. B* **14**(1), 144–154 (1997).
39. X. Liu and M. Pang, “Revealing the Buildup Dynamics of Harmonic Mode-Locking States in Ultrafast Lasers,” *Laser Photonics Rev.* **13**(9), 1800333 (2019).
40. V. A. Ribenek, D. A. Korobko, A. A. Fotiadi, *et al.*, “Supermode noise mitigation and repetition rate control in a harmonic mode-locked fiber laser implemented through the pulse train interaction with co-lased CW radiation,” *Opt. Lett.* **47**(19), 5236–5239 (2022).
41. D. A. Korobko, V. A. Ribenek, P. A. Itrin, *et al.*, “Polarization maintaining harmonically mode-locked fiber laser with suppressed supermode noise due to continuous wave injection,” *Opt. Laser Technol.* **162**, 109284 (2023).
42. V. A. Ribenek, D. A. Stoliarov, D. A. Korobko, *et al.*, “Mitigation of the supermode noise in a harmonically mode-locked ring fiber laser using optical injection,” *Opt. Lett.* **46**(22), 5747–5750 (2021).
43. C. Yang, B. Yao, Y. Chen, *et al.*, “570 MHz harmonic mode-locking in an all polarization-maintaining Ho-doped fiber laser,” *Opt. Express* **28**(22), 33028–33034 (2020).
44. Y. Zhang, K. Wu, Z. Guang, *et al.*, “Advances and Challenges of Ultrafast Fiber Lasers in 2–4 μm Mid-Infrared Spectral Regions,” *Laser Photonics Rev.* **18**(3), 2300786 (2024).
45. S. A. Filatova, V. A. Kamynin, N. R. Arutyunyan, *et al.*, “Comparison of mode-locking regimes in a holmium fibre laser,” *Quantum Electron.* **48**(12), 1113–1117 (2018).
46. L. Jin, Q. Zhang, B. Zhang, *et al.*, “Numerical analysis of hybrid mode-locking stability in a Ho-doped fiber laser,” *Opt. Express* **31**(2), 1141–1153 (2023).
47. S. Wang, R. Zhou, H. Liu, *et al.*, “Influence of saturable absorber parameters on the hybrid mode-locking performance of fiber lasers,” *J. Appl. Phys.* **134**(5), 053104 (2023).
48. A. S. Kurkov, “Oscillation spectral range of Yb-doped fiber lasers,” *Laser Phys. Lett.* **4**(2), 93–102 (2007).
49. M. Pawliszewska, T. Martynkien, A. Przewłoka, *et al.*, “Dispersion-managed Ho-doped fiber laser mode-locked with a graphene saturable absorber,” *Opt. Lett.* **43**(1), 38–41 (2018).
50. A. G. Nasibulin, A. Kaskela, K. Mustonen, *et al.*, “Multifunctional Free-Standing Single-Walled Carbon Nanotube Films,” *ACS Nano* **5**(4), 3214–3221 (2011).
51. Y. Tian, A. G. Nasibulin, B. Aitchison, *et al.*, “Controlled Synthesis of Single-Walled Carbon Nanotubes in an Aerosol Reactor,” *J. Phys. Chem. C* **115**(15), 7309–7318 (2011).
52. E. M. Khabushev, D. V. Krasnikov, O. T. Zaremba, *et al.*, “Machine Learning for Tailoring Optoelectronic Properties of Single-Walled Carbon Nanotube Films,” *J. Phys. Chem. Lett.* **10**(21), 6962–6966 (2019).
53. A. Kaskela, A. G. Nasibulin, M. Y. Timmermans, *et al.*, “Aerosol-Synthesized SWCNT Networks with Tunable Conductivity and Transparency by a Dry Transfer Technique,” *Nano Lett.* **10**(11), 4349–4355 (2010).
54. D. Galiakhmetova, Y. Gladush, A. Mkrtychyan, *et al.*, “Direct measurement of carbon nanotube temperature between fiber ferrules as a universal tool for saturable absorber stability investigation,” *Carbon* **184**, 941–948 (2021).
55. G. Sobon, “Mode-locking of fiber lasers using novel two-dimensional nanomaterials: graphene and topological insulators [Invited],” *Photonics Res.* **3**(2), A56 (2015).
56. J. Wu, D. Y. Tang, L. M. Zhao, *et al.*, “Soliton polarization dynamics in fiber lasers passively mode-locked by the nonlinear polarization rotation technique,” *Phys. Rev. E* **74**(4), 046605 (2006).
57. D. A. Korobko, V. A. Ribenek, D. A. Stoliarov, *et al.*, “Resonantly induced mitigation of supermode noise in a harmonically mode-locked fiber laser: revealing the underlying mechanisms,” *Opt. Express* **30**(10), 17243–17258 (2022).
58. J. Jeon, J. Lee, and J. H. Lee, “Numerical study on the minimum modulation depth of a saturable absorber for stable fiber laser mode locking,” *J. Opt. Soc. Am. B* **32**(1), 31–37 (2015).
59. J. Lee, S. Kwon, and J. H. Lee, “Numerical Investigation of the Impact of the Saturable Absorber Recovery Time on the Mode-Locking Performance of Fiber Lasers,” *J. Lightwave Technol.* **38**(15), 4124–4132 (2020).
60. M. Chernysheva, A. Rozhin, Y. Fedotov, *et al.*, “Carbon nanotubes for ultrafast fibre lasers,” *Nanophotonics* **6**(1), 1–30 (2017).

61. W. S. Man, H. Y. Tam, M. S. Demokan, *et al.*, "Mechanism of intrinsic wavelength tuning and sideband asymmetry in a passively mode-locked soliton fiber ring laser," *J. Opt. Soc. Am. B* **17**(1), 28–33 (2000).
62. C. R. Menyuk, "Stability of solitons in birefringent optical fibers II Arbitrary amplitudes," *J. Opt. Soc. Am. B* **5**(2), 392–402 (1988).
63. M. N. Islam, C. D. Poole, and J. P. Gordon, "Soliton trapping in birefringent optical fibers," *Opt. Lett.* **14**(18), 1011–1014 (1989).